Innovative Application of Statistical Sound Analysis for Fault Diagnosis in Variable-Speed Induction Machines

Abderrahman El idrissi[1,*], Aziz Derouich[1], Said Mahfoud[2], Najib El ouanjli[3], Hamid Chojaa[1] and Ahmed Chantoufi[1]

[1] Industrial Technologies and Services Laboratory, Higher School of Technology, Sidi Mohamed Ben Abdellah University, Fez 30000, Morocco

[2] Polydisciplinary Laboratory of Sciences, Technologies, and Societies, Higher School of Technology, Sultan Moulay Slimane University, Khenifra 54000, Morocco

[3]Laboratory of Mechanical, Computer, Electronics and Telecommunications, Faculty of Sciences and Technology, Hassan First University, Settat 26000, Morocco

*Corresponding author: Abderrahman El Idrissi (abderrahman.elidrissi1@usmba.ac.ma)

Abstract. The article presents an innovative method leveraging statistical sound analysis to diagnose malfunctions in variable-speed drive-controlled (VSD) induction machines (IM). This early anomaly detection approach strengthens preventive maintenance by preventing major failures. The bell-shaped curve of the Gaussian distribution, integrated into this analysis, reveals a significant concentration of values around the mean, thus facilitating the early detection of abnormal sounds emitted by the machine. Experiments highlight that driving IMs controlled by frequency inverters at low speeds can induce the emergence of resonance frequencies, altering the machine's sound in an unusual and bothersome manner. To address this issue, a statistical characterization of the sound data from IMs is adopted. In this experimental study, the machine is first powered by a zero-frequency inverter, then by frequencies of 16.66Hz, 33.33Hz, and finally at the nominal frequency of 50Hz. The recorded sound signals are then transformed in to data matrices, and a statistical analysis is conducted, calculating different variables and coefficients of high-order statistics (HOS). This approach leads to precise characterization of normal and abnormal sounds, thus improving the machine's reliability and overall operational efficiency.

Keywords. Diagnosis, Induction Machine, Variable-speed drive-controlled, statistical sound analysis.

1. Introduction

Electromechanical drive represents a crucial domain in the industry, where Induction machines (IMs) hold a prominent position due to their robustness and low maintenance requirements [1–6]. However, despite their undeniable advantages, these machines generate a significant level of noise [7–9].

A stator and a rotor are the two major parts of an electric motor; the air gap is the space between the two. The end shields, the housing, the shaft, and the cooling system—which may include parts like fans or water jackets—are a few more important factors that need to be considered. Considering all of this, we may differentiate between three primary categories of noise sources: mechanical, electromagnetic, and aerodynamic [10].

The magnetic field in the air gap is the primary source of electromagnetic noise, also known as electrical noise, from electric motors. Bearings, rotor-stator eccentricity, and mechanical unbalance are the primary sources of mechanical noise. Lastly, the noise generated by the motor's cooling and ventilation system is known as aerodynamic noise. As a result of electric motors that are powered by electronic converters, some publicationsalso distinguish noise of electronic origin [11].

The radial distribution of forces on the machine structure is the primary source of vibration and electromagnetic noise. The flux is dispersed both tangentially and radially when the stator is subjected to the alternating current source [12]. Under both load and no-load situations, the magnetic field in the air gap produces the radial flux distribution [13]. There are several higher-order harmonics in the air-gap field, which produce electromagnetic noise and vibrations

[14]. Electromagnetic noise and vibration are caused by air-gap harmonics, which produce harmonics in Maxwell's radial force. The opening of the rotor and stator slots generates harmonics in the permeance of the air gap. These effects are also influenced by magnetic saturation of the core, current-time harmonics in the stator winding, the magnetostriction process caused by the inverter, and rotor and stator eccentricity due to manufacturing errors [15].

Over the years, the usage specifications of these machines have evolved, particularly with the increasing introduction of power electronics for their operation.

In this context, research efforts primarily focus on two fronts: the optimized design of electric actuators and the complex interaction between power electronics and electric machines. Static converters offer more precise control, but they also give rise to noise and vibration issues, particularly those attributed to "magnetic origin noise" [8, 16].

With increasingly stringent acoustic standards, particularly in the transportation sector, it has become essential to master the understanding and prediction of electromagnetic noise in variable regimes. Pulse width modulation (PWM) strategies introduce a multitude of temporal harmonics into the spectrum of electromagnetic forces, stimulating the stator structure and increasing the risk of resonance, leading to vibration and IM overheating. Much research is devoted to addressing the issue of reducing rotating electrical machines controlled by PWM inverters. However, noise reduction cannot be tackled in isolation. It necessitates a multidisciplinary approach involving specialists from various domains such as electronic controls, electromechanics, and acoustics [8, 9].

In the realm of fault diagnosis of electric machines, particular attention is given to the acquisition and processing of sounds and noises emitted by IMs to detect faults, especially mechanical ones like bearing defects [17]. A common approach to monitor phenomena such as friction occurring in large rotating machines is to use the acoustic emission (AE) method by acquiring, analyzing, and processing signals. For instance, authors in [18] developed a cross-correlation method based on AE to locate friction zones in a rotorbearing system using wavelet analysis. Additionally, these authors employed Kolmogorov-Smirnov statistics in acoustic emission technology to describe the types of shaft seal friction and localize their position by Time Difference Of Arrival (TDOA). Induction motors emit various types of noises that overlap, making their separation complex. To address this challenge, a noise source separation method based on Adaptive Scale-Space Modal Extraction (ASSME) is proposed in [9].

The challenge sometimes lies in the need to operate the IM at low speeds, which can jeopardize its safety if operated for extended periods due to inverter frequency. Therefore, it is crucial to characterize the AEs of this IM and determine thresholds not to exceed to preserve its normal operating state. Recent work on the acquisition and classification of sounds and acoustic noises emanating from the IM relies on intelligent classification algorithms [19, 20], but these methods require extensive testing in different scenarios, for IMs of various powers, and in the presence of different anomalies [21]. Hence, many classification algorithms rely on statistical learning. Descriptive statistics can be an effective alternative for characterising the acoustic emissions for each operating state by estimating the impact of the variation in frequency imposed by the variable speed drive using statistical parameters and metrics. This method has recently been used to estimate the impact of stator imbalance on the noise of three-phase asynchronous machines [22].

In this perspective, this work seeks to adopt a statistical approach by leveraging the Gaussian normal law and various significant statistical parameters to identify and measure abnormal noise from the IM when controlled by a PWM-based VSD.

The results obtained have demonstrated the necessity of operating the IM at a speed closer to synchronous speed, and we have estimated the critical values of the different statistical parameters involved, as well as the two parameters, signal-to-noise ratio (SNR) and total harmonic distortion (SINAD), which should be negative under normal operation.

This article is organized as follows: Section 2 presents a brief explanation of the origin of IM noise, Section 3 describes the experimental setup, materials used, and the adopted methodology, Section 4 presents the results obtained and their interpretation, and finally, Section 5 concludes the work.

2. The Induction machine sound

Each component of rotating electrical machines contributes in its own way to the generation of sound emitted by these machines, whether through electromagnetic interactions, mechanical vibrations, or friction [23].

Structural vibrations are caused by forces produced by electromagnetic fields. The forces' amplitudes and, most importantly, their frequencies determine how much the system vibrates; these frequencies don't have to match the system's inherent frequencies. The vibratory energy is subsequently transformed into sound energy by these surface vibrations.

In electrical machinery, electromagnetic noise is caused by two different kinds of forces: Maxwell forces and magnetostriction forces. Since radial vibration waves from the yoke (circumferential modes) are typically the most efficient in radiating acoustic noise, they are the primary structural modes of importance for acoustic noise in radial flux rotating machines. The stator yoke may deflect radially due to magnetostriction and Maxwell forces [24].

The radial force per unit area obtained from Maxwell's tensor is given by equation (1) [12] :

$$F = \frac{B^2{}_r - B^2{}_t}{2\mu_0} \qquad (1)$$

where μ_0 ($4\pi.10^{-7}Hm^{-1}$) is the vacuum's magnetic permeability, B_r is the magnetic flux's radial component, B_t is its tangential component, and F is its force per unit area. The motor emits noise into the surrounding environment as a result of vibrations in the stator caused by the radial force produced inside the motor.

Efficient management of the noise emitted by IMs is of crucial importance to improve the environmental impact and acoustic comfort of electrical machines in various industrial and commercial applications. The distinctive characteristics of the sound and noise emitted by induction machines are primarily linked to their specific design as well as their electromagnetic and mechanical aspects [25, 26]. These aspects are often influenced by the nature of the three-phase electrical supply, especially when powered by PWM-based VSD [16, 23, 25, 27]. Figure 1 provides a general illustration of the source and process of magnetic noise generation in the IM.

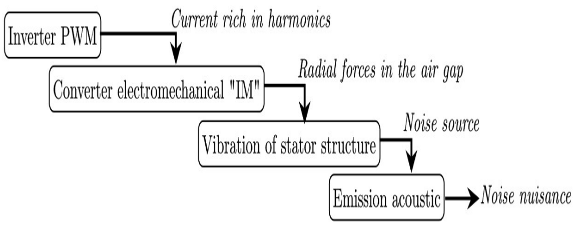

Fig. 1. Process of magnetic noise induction in the IM

This diagram in Figure 1 illustrates the direct relationship between the quality of the power supply and the acoustic noise emitted by the motor; in particular, it shows that the harmonics generated by the PWM control can generate acoustic nuisance via a chain of electromechanical interactions. This representation is particularly relevant for assessing the merits of optimising the control strategy, filtering or mechanical design of the motor to reduce noise emissions.

3. EXPERIMENTAL BENCH

This experimental work is based on the study of a 1.5 kW induction machine (IM) powered by a three-phase frequency converter. The inverter allows precise control of the machine's operating frequency, and therefore its rotational speed.

Initially, the IM was powered at zero frequency. In this case, the machine obviously remains at zero speed (0 rpm), but nevertheless emits a perceptible noise that is noticeably high and potentially nuisance-producing. The frequency was then increased: first to 16.66 Hz (approximately 500 rpm), then to 33.33 Hz (approximately 1000 rpm). These two frequencies correspond to low-speed regimes that the manufacturer generally advises against, as they can lead to degraded acoustic and mechanical performance. Finally, a test was carried out at the nominal frequency of 50 Hz, corresponding to the synchronous speed of 1500 rpm.

The aim of this series of tests was to analyse the influence of the power supply frequency on the acoustic signature of the machine, and more specifically to observe changes in noise emissions as a function of speed. Figure 2 shows the block diagram of the setup.

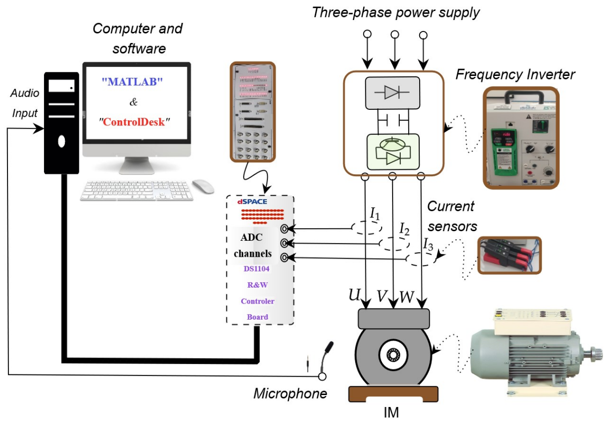

Fig. 2. Block diagram of the setup

Thus, the experimental setup contains the elements as shown in Figure 3.

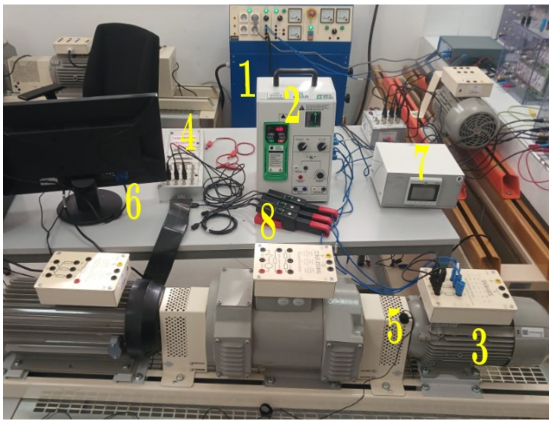

Fig. 3. The experimental setup elements

Table 1 lists the names of the numbered components of the experimental setup.

Table 1. Identification of the components of the experimental device

Number	Description	Number	Description
1	Three-phase power source 400V	5	Microphone
2	Three-phase VSD	6	Computer
3	IM	7	Station for measuring electrical quantities
4	Interface card dSPACE	8	Current sensors

The main elements of the experimental test bench shown in Table 1 are: the IM tested with the variable frequency drive, which has a four-position switch for the four speeds (0rpm, 500Rpm, 1000Rpm and 1500Rpm), and the measuring station for the electrical quantities (voltage, current, power factor and active power), In addition, three current sensors to monitor three-phase current signals in real time in the control desk at the DSPACE 1104 interface. The last key element is the microphone, which captures the sound of the IM and displays it in the MATLAB environment.

The nominal characteristics of the IM are provided in Table III in the appendix. Additionally, the sound of the IM is captured by a directional microphone, placed near the IM. This microphone is directly connected to the computer's audio input, as demonstrated in the previous figure 2, under quiet laboratory conditions. The main characteristics of the microphone used are given in table VI in the appendix.

In the MATLAB environment, we utilize an application called "Audio-Labler" to record various sound samples of the IM in different situations. These audio samples, with the extension "*.wav", are then converted into MATLAB data matrices ".mat" for further processing.

Regarding the IM current signals, they are captured by current sensors as illustrated in Figures 2 and 3. To display the signals on the computer in the "Control Desk" environment.

4. Results and discussions

The sound data extracted in the five operating situations of the IM, namely direct feeding (DF) at a frequency of 50 Hz, feeding by variable frequency with f=0 Hz, f=16.66 Hz, f=33.33 Hz, and f=50 Hz, are statistically analyzed using three tools: the Gaussian curve, box plots to clearly distinguish normal and abnormal acoustic data. These results will illustrate the impact of VFDs and low-speed operation on the sound emitted by the IM and determine situations where the IM poses an increased risk. The quantification of the abnormality of the IM's state will be described using three statistical coefficients: Root Mean Square (RMS), Crest Factor (CF), Impulse Factor (IF), Kurtosis (K) [28], as well as two other popular signal processing factors to quantify the performance of the IM from its sound, which are SINAD (Signal-to-Noise and Distortion Ratio) and SNR (Signal-to-Noise Ratio) [29]. These parameters are given by the following equations.

$$RMS = \sqrt{\frac{\sum_{i=1}^{n}(x_i)^2}{n}} \tag{2}$$

$$CF_x = \frac{\hat{x}}{\sqrt{\frac{\sum_{i=1}^{n}(x_i)^2}{n}}} \tag{3}$$

$$IF_x = \frac{\hat{x}}{\sqrt{\frac{\sum_{i=1}^{n}|x_i|}{n}}} \tag{4}$$

$$K = \frac{1}{\sigma^4}\frac{\sum_{i=1}^{n}(x_i-\mu)^4}{n} \tag{5}$$

$$SINAD = 20\log\left(\frac{\text{Signal}}{\text{Noise}+\text{Distortion}}\right) \tag{6}$$

$$SNR = 20\log\left(\frac{\text{Signal}}{\text{Noise}}\right) \tag{7}$$

- RMS: It represents the quadratic mean of the values of an alternating signal, establishing a relationship between the maximum value and the effective value of the signal.
- CF: It is the peak value divided by the RMS value. Defects often first manifest as changes in the peak value of a signal before manifesting in the energy represented by the RMS. The crest factor can provide early warning for defects as they first develop.
- IF: It compares the height of a peak to the average level of the signal.
- Kurtosis: It provides information about the distribution of data by emphasizing values that are far from the mean.

- SNR: It quantifies the proportion of the signal to the noise, while SINAD evaluates the proportion of the signal to the sum of the noise and distortion.

In this context, it is crucial to interpret these two signal processing factors properly, and since electromagnetic sound dominates over mechanical noise, the latter is considered as noise while electromagnetic noise represents the signal.

Therefore, in our case, the normal values of these two signal processing parameters should be negative and close to zero. A negative value, far from zero, indicates that the IM exhibits mechanical vibrations caused by PWM control.

The values of these statistical and signal processing parameters obtained under healthy conditions serve as reference points. Any deviation from these values indicates a malfunction in the machine, potentially caused by a variation in the supply frequency, which must be kept at an appropriate level.

Before embarking on the statistical analysis of the acoustic data, it is essential to present these signals in the time and frequency domains.

4.1 Acoustic signals in the time and frequency domain

According to Figure 4, the amplitudes are distinguished in both domains. It is observed that the sound emitted during low-speed operation dominates other sounds during synchronous speed operation or at standstill (f=0Hz). Also, in the time domain for frequencies (16.66Hz, 33.33Hz), the amplitudes reach a quite disturbing level exceeding the saturation values given by the microphone [-1,1].

The signals in green and blue correspond to the normal operation of the IM without any danger (f=50Hz), with additional noise in the case of VSD (blue signal). On the other hand, the three other signals indicate a risk for the IM if it operates for an extended period.

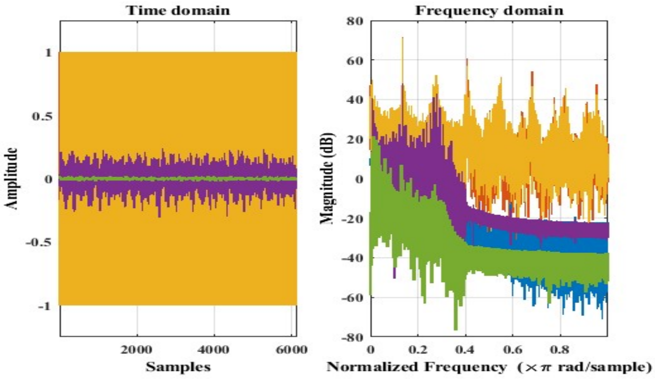

Fig. 4. The sound signals in the time and frequency domains

Although Figure 4 presents the amplitudes of the sound signatures in the time and frequency domains, it is essential to underline the normality of these signatures by conducting a statistical study of the acoustic data.

4.2 Acoustic data desciption using the Gaussian curve

In the figure below (Figure 5), the Gaussian curve represents the acoustic behavior of the IM when controlled by a PWM inverter. In Figure 5a, the data is almost normal, the shaded part corresponds to mechanical noise, and the data align with the ideal curve. This similarity between Figure 5a and Figure 5e indicates that when the IM is supplied with nominal frequency voltage (50Hz), its noise is normal, and there is no risk in this case.

In cases where the noise is abnormal, as illustrated by Figures 5b, 5c, and 5d, the data is distributed without matching the ideal curve, especially with frequencies of 16.66 Hz and 33.33 Hz (Figure 5c and 5d), where the magnetic noise is disturbing and masks the mechanical sound of the IM. Furthermore, in the case of Figure 5b, the data is almost normal with an absence of mechanical noise (IM at standstill), but the amplitude of this noise is far from normal.

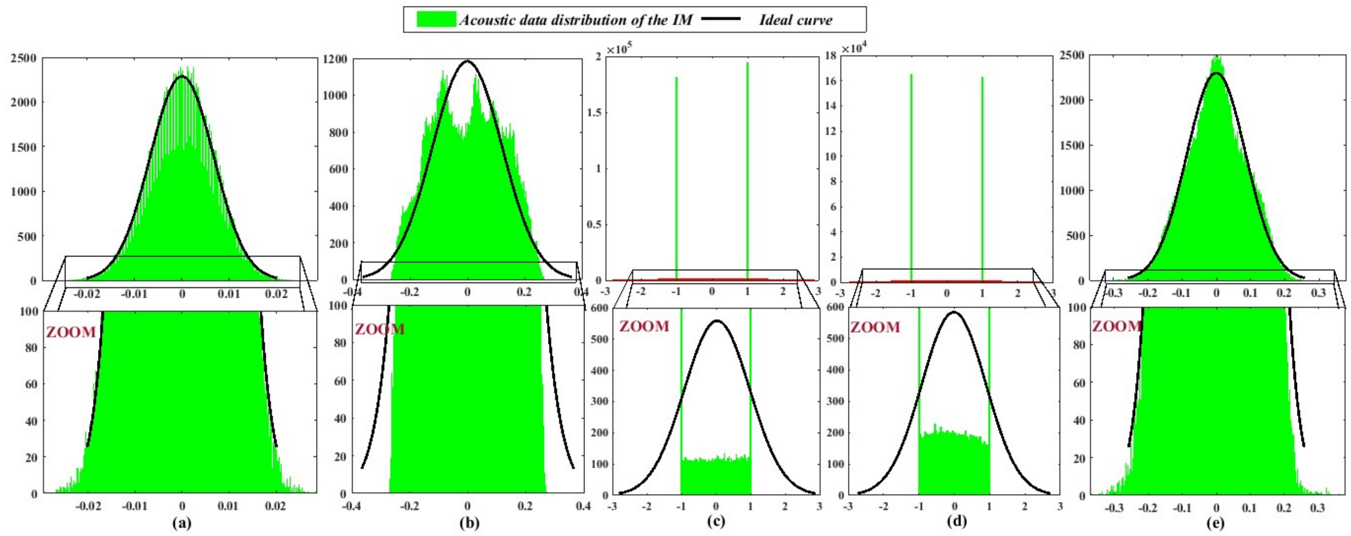

Fig. 5. The histograms represent the distribution of sound data in different situations: (a) No load - Healthy, (b) with VSD_0 Hz, (c) with VSD_16.66 Hz, (d) with VSD_33.33 Hz, (e) with VSD_50 Hz.

The observations from Fig.5 are corroborated by the following Fig.6. Indeed, the boxplots corresponding to each operating mode clearly illustrate the distribution of acoustic data.

4.3 Acoustic data desciption using the box plot

The box plot is a graphical tool used to summarize the distribution of a dataset based on key quantiles. It consists of several components [22, 30] Figure 6 shows the box plot structure:

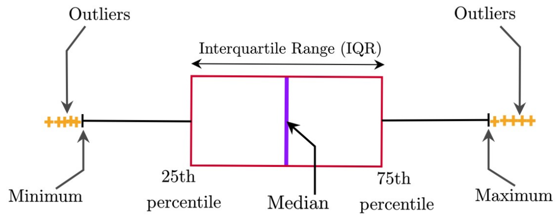

Fig. 6. Box plots description

- The dataset is divided into two equal halves by the median value, which is represented by the median line inside the box.
- The interquartile range (IQR) is the range between the 25th and 75th percentiles (quartiles), which are represented by the box's edges.
- The whiskers, which represent the predicted distribution of the data, extend beyond the box by up to 1.5 times the IQR. A point is indicated separately if it falls outside of this range, which is regarded as an outlier.

According to Figure 7, in the case of a 50 Hz frequency from a DF three-phase source, we observe a normal distribution of data, with an amplitude not exceeding 0.005 and the median located at the center of the box. When using a frequency inverter with a frequency of 50 Hz, the noise remains normal, but it is noteworthy that the magnetic noise (ten times higher compared to DF) as well as the mechanical noise increase, as evidenced by the amplitude of the box and the presence of outlier points in red, representing mechanical noise.

The box plot corresponding to the noise at 0 Hz shows significant magnetic noise, surpassing that of VSD-50 Hz, with an absence of mechanical noise, of course. For the other two cases (16.66 Hz and 33.33 Hz), we observe a shift of the median, which should ideally divide the box into two equal halves in the case of normal operation. Furthermore, the large amplitude of the boxes highlights the danger of operating in this regime, where magnetic noise dominates over mechanical noise.

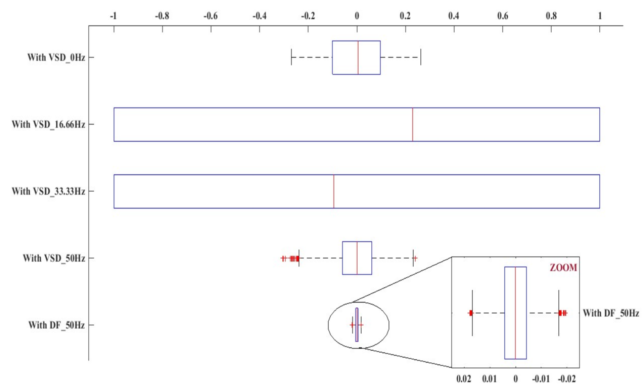

Fig. 7. Assessment of the normality of sounds emitted by the IM using boxplot diagrams.

4.4 Acoustic data desciption using the QQ-plot

The QQ-plot (Quantile-Quantile plot), also known as the probability plot, is a graphical tool used to visually judge whether a data sample follows an adopted theoretical distribution, in particular the normal distribution. In this type of plot, the position of the empirical quantiles of the dataset is related to the position of the corresponding quantiles of a reference distribution, in this case the normal distribution. If the dataset follows the chosen distribution, all the points on the graph are aligned approximately on a straight line: the normality line. A good alignment of all the points shows that the data set has a distribution close to that of the postulated law, while deviations from this line indicate the existence of deviations from the law, such as asymmetries, kurtosis or the presence of a certain number of extreme values (outliers).

The probability plot is therefore a simple, intuitive and rapid tool for an initial presentation of the normality hypothesis, or for revealing abnormal behaviour in the data from a sample (See Figure 8).

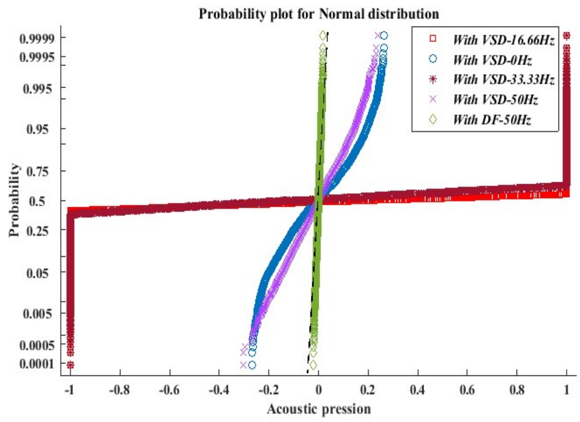

Fig. 8. Assessment of the normality of sounds emitted by the IM using probability plot.

The figure 8 above shows the probability plot of an evaluation of the conformity of sound pressure data to a normal distribution, for different power supply regimes of an induction motor. The tests carried out are with different frequencies stimulated by the variable speed drive (VSD): 0 Hz, 16.66 Hz, 33.33 Hz, 50 Hz, and with a direct supply (DF) at 50 Hz.

The order in which the experimental samples are placed in relation to the reference line (dotted line) shown in the graph indicates the level of normality achieved by the data. Conversely, the fewer the points aligned with this line, the more the distribution is not considered normal. The analysis showed that the distribution obtained under DF at 50 Hz is the one with the best fit to the normal distribution, which is synonymous with stable acoustic behaviour. The cases with VSD at 0 Hz and 50 Hz imposed by the VSD are also close, with a clear illustration that at 50Hz imposed by the drive is closer to normal than that at 0Hz (0 Rpm).

The data collected at the frequencies of 16.66 Hz and 33.33 Hz are, on the other hand, very distant from normal, which is synonymous with non-Gaussianity, probably because there are unstable dynamics or non-uniformities in low-frequency operation. This also shows and confirms the effect of low frequencies on the motor's acoustic signature and subsequently on its vibratory behaviour.

4.5 Estimating the normality of acoustic data using statistical parameters

The parametric estimation of these operating modes relies on the use of statistical parameters and the calculation of the signal-to-noise and distortion ratio described and provided in equations 1 to 5. The obtained values are presented through the graphs in Figures 9 and 10.

Indeed, a normal acoustic behavior corresponds to an almost zero RMS value, while abnormal acoustic signals related to low-speed operation of the IM have an RMS approaching 1. This parameter is also correlated with the amplitude of the acoustic signals, as illustrated in Figure 9.

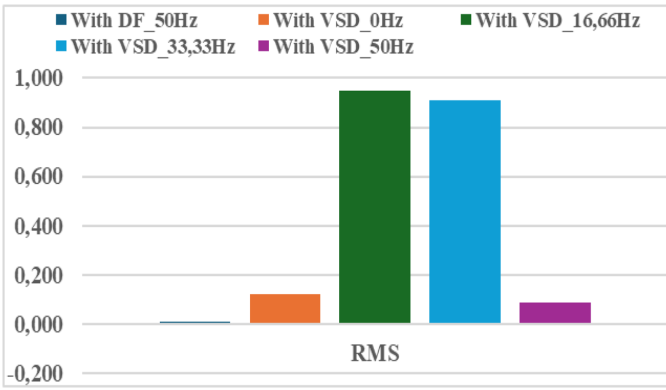

Fig. 9. RMS of acoustic data from the IM.

The other statistical parameters (CF, IF, and Kurtosis) in Figure 10 clearly reveal the most abnormal operating states, corresponding to 16.66 Hz and 33.33 Hz, or 500 rpm and 1000 rpm, respectively, where IF, CF, and Kurtosis reach 1, meaning that the maximum amplitude equals the mean. This situation represents a high risk for the IM if it operates for an extended period. Furthermore, applying zero-frequency voltage to the IM produces parameter values almost equal to 2, as indicated in Table II. In contrast, under normal conditions, the values are approximately CF=4.4 and IF=5.5, with a kurtosis coefficient of 3, which is considered ideal.

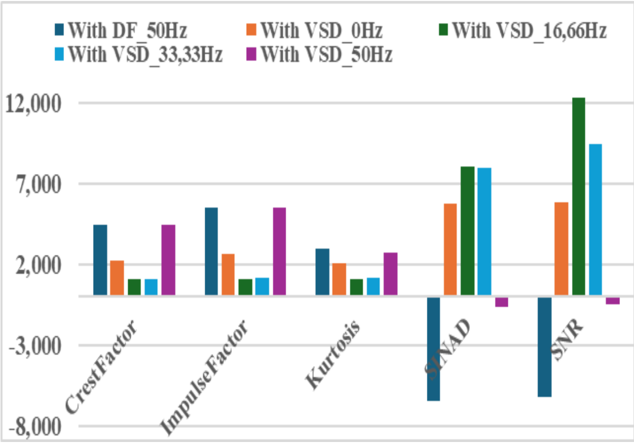

Fig. 10. Measurement of the sound quality of the IM using statistical parameters.

To prove and confirm the normality or abnormality of the acoustic emissions from our IM, the signal processing parameters SINAD and SNR clearly distinguish between normal and abnormal sounds. In abnormal states (0 Hz, 16.66 Hz, and 33.33 Hz), the SNR and SINAD values are positive, exceeding 12, while normal states (50 Hz) are characterized by negative values. Moreover, with DF_50Hz, these two parameters are around -6.5, indicating the absence of abnormal noise. Whereas, with the use of the frequency inverter (With VSD_50Hz), they are close to -0.5, indicating the impact of harmonic injection into the current by this power electronics inverter.

From the graphical results (such as the Gaussian curve and box plot) and parametric results (including RMS and other statistical factors), it is evident that this statistical analysis provides valuable insights into the health condition and performance assessment of the IM. The Gaussian curve helps visualize the distribution of temperature data and identify deviations from normal operation, while the box plot highlights data dispersion and the presence of potential outliers, indicating abnormal conditions.

The parametric values, such as RMS, and kurtosis, quantify these variations and allow for a more precise estimation of the motor's operating state. Together, these graphical and parametric results enable a comprehensive evaluation of the motor's health, making it possible to detect anomalies early on and ensure optimal performance. The Table 2 summarises the values obtained.

Table 2. The values of the statistical parameters, SINAD and SNR

State	CF	Impulse Factor	Kurtosis	SINAD	SNR	RMS
With DF_50Hz	4,395	5,478	2,914	-6,488	-6,258	0,007
With VSD_0Hz	2,248	2,641	2,051	5,769	5,822	0,122
With VSD_16,66Hz	1,054	1,080	1,090	8,009	12,285	0,949
With VSD_33,33Hz	1,101	1,152	1,163	7,931	9,417	0,909
With VSD_50Hz	4,402	5,491	2,697	-0,624	-0,505	0,086

The data presented in Table 2 highlights the strong dependence of the acoustic signal quality on the power supply frequency. Low frequencies (16.66 Hz and 33.33 Hz) provide highly impulsive, noisy and asymmetrical signals, whereas 50 Hz regimes (direct supply or via VSD) result in a more stable, regular signal that is close to Gaussian behaviour. These observations confirm the value of using statistical indicators to characterise the operating state of the machine and detect potentially acoustically harmful regimes.

5. Conclusion

The sound emitted by an IM provides crucial information about its operating condition. With the use of frequency converters to drive these machines at lower speeds, it has become essential to characterize the abnormal sounds emitted by the IM. This article describes an approach based on statistical analysis and signal processing to distinguish between normal and abnormal sounds, thereby indicating the thresholds necessary to stop or adjust the speed of the IM. Gaussian curves, QQ-plot and boxplots enable a visual distinction of the different operating states. The results obtained for various parameters show clearly defined thresholds for normal and abnormal operation, especially for SNR and SINAD, which should be negative for nearly ideal operation, reaching around -6 for both parameters. kurtosis, CF and IF values that are almost equal to 1 also indicate an abnormal sound from the IM. Future research perspectives will focus on diagnosing stator imbalance defects caused either by supply voltage imbalance or by short circuits between coils. This will be achieved through intelligent analysis of acoustic signals, utilizing statistical learning algorithms.

Appendix

Table 3. The IM Parameters

Variable	Symbol	Value (unit)
Nominal power	P_m	1.5 kW
Nominal stator voltage	U_{sn}	400 V
Frequency	f	50 Hz
Pair pole number	p	2

Table 4. Specification of the microphone used for sound acquisition.

Parameters	Values and specifications
Model	Microphone Candc DC-C6 Lavalier
Type	Unidirectional microphone with noise suppression function
Sensitivity	-46 ± 2db
Operating voltage	DC1.0V-10 V
Frequency response	65 Hz à 18 kHz

References

[1] Blodt, M., Granjon, P., Raison, B., & Rostaing, G. (2008). Models for bearing damage detection in induction motors using stator current monitoring. IEEE transactions on industrial electronics, 55(4), 1813-1822. https://doi.org/10.1109/TIE.2008.917108.

[2] Saucedo-Dorantes, J. J., Jaen-Cuellar, A. Y., Perez-Cruz, A., & Elvira-Ortiz, D. A. (2023). Detection of inter-turn short circuits in induction motors under the start-up transient by means of an empirical wavelet transform and self-organizing map. Machines, 11(10), 958. https://doi.org/10.3390/machines11100958.

[3] El Idrissi, A., Derouich, A., & Mahfoud, S. (2022, January). Fault diagnosis of the bearing outer ring of an induction motor under DTC control by using Hilbert filter. In International Conference on Digital Technologies and Applications (pp. 802-812). Cham: Springer International Publishing. https://doi.org/10.1007/978-3-031-01942-5_80.

[4] A. El Idrissi, A. Derouich, and S. Mahfoud, Fault Diagnosis of the Bearing Outer Ring of an Induction Motor Under DTC Control by Using Hilbert Filter, vol. 454 LNNS. 2022. https://doi.org/10.1007/978-3-031-01942-5_80.

[5] El Idrissi, A., Derouich, A., Mahfoud, S., El Ouanjli, N., Chantoufi, A., Al-Sumaiti, A. S., & Mossa, M. A. (2022). Bearing fault diagnosis for an induction motor controlled by an artificial neural network—Direct torque control using the Hilbert transform. Mathematics, 10(22), 4258. https://doi.org/10.3390/math10224258.

[6] Chantoufi, A., Derouich, A., El Ouanjli, N., Mahfoud, S., El Idrissi, A., & Taoussi, M. (2023, January). Direct torque control for doubly fed induction motor driven electric vehicle. In International Conference on Digital Technologies and Applications (pp. 862-871). Cham: Springer Nature Switzerland. https://doi.org/10.1007/978-3-031-29860-8_86.

[7] Van Brandt, L., Silveira, F., Delvenne, J. C., & Flandre, D. (2023). On noise-induced transient bit flips in subthreshold SRAM. Solid-State Electronics, 208, 108715. https://doi.org/10.1016/j.sse.2023.108715.

[8] Le Besnerais, J. (2008). Reduction of magnetic noise in PWM-supplied induction machines-low-noise design rules and multi-objective optimization (Doctoral dissertation, Ecole Centrale de Lille).

[9] Wang, Z., Gu, Y., Chen, C., Wang, L., & Sun, X. (2023). Induction motor noise source separation and identification based on adaptive scale-space mode extraction. Machines, 11(4), 449. https://doi.org/10.3390/machines11040449.

[10] Gonzalez, P., Buigues, G., & Mazon, A. J. (2023). Noise in electric motors: A comprehensive review. *Energies*, *16*(14), 5311. https://doi.org/10.3390/en16145311.

[11] Vijayraghavan, P., & Krishnan, R. (1999). Noise in electric machines: A review. IEEE Transactions on Industry Applications, 35(5), 1007-1013. https://doi.org/10.1109/28.793360

[12] Gieras, J. F., Wang, C., & Lai, J. C. (2018). Noise of polyphase electric motors. CRC press. https://doi.org/10.1201/9781420027730.

[13] Dajaku, G., & Gerling, D. (2009, May). Magnetic radial force density of the PM machine with 12-teeth/10-poles winding topology. In 2009 IEEE International Electric Machines and Drives Conference (pp. 1715-1720). IEEE. https://doi.org/10.1109/IEMDC.2009.5075434.

[14] Le Besnerais, J., Lanfranchi, V., Hecquet, M., Romary, R., & Brochet, P. (2009). Optimal slot opening width for magnetic noise reduction in induction motors. IEEE Transactions on Energy Conversion, 24(4), 869-874. https://doi.org/10.1109/TEC.2009.2025421.

[15] Khan, M. A., Khan, F., Rahman, L. U., & Fatima, A. (2018, November). Analysis and electromagnetic noise suppression of three-phase squirrel cage induction motor. In 2018 International Conference on Computing, Electronic and Electrical Engineering (ICE Cube) (pp. 1-5). IEEE. https://doi.org/10.1109/ICECUBE.2018.8610983.

[16] Marignetti, F., Rubino, G., Boukadida, Y., Conti, P., De Gregorio, F., Iengo, E., & Longobardi, V. G. (2020, June). Noise and vibration analysis of an inverter-fed three-phase induction motor. In 2020 International Symposium on Power Electronics, Electrical Drives, Automation and Motion (SPEEDAM) (pp. 157-161). IEEE. https://doi.org/10.1109/SPEEDAM48782.2020.9161859.

[17] Hou, Y., Zhou, C., Tian, C., Wang, D., He, W., Huang, W., ... & Wu, D. (2022). Acoustic feature enhancement in rolling bearing fault diagnosis using sparsity-oriented multipoint optimal minimum entropy deconvolution adjusted method. Applied Acoustics, 201, 109105. https://doi.org/10.1016/j.apacoust.2022.109105.

[18] Pan, Q., Zhou, R., Su, J., He, T., & Zhang, Z. (2019). Automatic localization of the rotor-stator rubbing fault based on acoustic emission method and higher-order statistics. Journal of Mechanical Science and Technology, 33, 513-524. https://doi.org/10.1007/s12206-019-0104-9.

[19] AlShorman, O., Alkahatni, F., Masadeh, M., Irfan, M., Glowacz, A., Althobiani, F., ... & Glowacz, W. (2021). Sounds and acoustic emission-based early fault diagnosis of induction motor: A review study. Advances in Mechanical Engineering, 13(2), 1687814021996915. https://doi.org/10.1177/1687814021996915.

[20] Alshorman, O., & Alshorman, A. (2021). A review of intelligent methods for condition monitoring and fault diagnosis of stator and rotor faults of induction machines. International Journal of Electrical & Computer Engineering (2088-8708), 11(4). https://doi.org/10.11591/ijece.v11i4.pp2820-2829.

[21] Verma, N. K., Sevakula, R. K., Dixit, S., & Salour, A. (2015). Intelligent condition based monitoring using acoustic signals for air compressors. IEEE Transactions on Reliability, 65(1), 291-309. https://doi.org/10.1109/TR.2015.2459684.

[22] El Idrissi, A., Derouich, A., Mahfoud, S., El Ouanjli, N., Chantoufi, A., & El Mourabit, Y. (2025). Acoustic characterization of a three-phase asynchronous machine under stator unbalance defects. *e-Prime-Advances in Electrical Engineering, Electronics and Energy*, *12*, 100958. https://doi.org/10.1016/j.prime.2025.100958.

[23] Zheng, X., Sun, Y., Yu, Y., Liu, C., & Qiu, Y. (2025). Prediction of Aerodynamic Noise of a Traction Induction Motor Using Methods of Computational Fluid Dynamics and Lighthill Acoustic Analogy. *Acoustics Australia*, 1-13. https://doi.org/10.1007/s40857-024-00344-w.

[24] Souron, Q., Le Besnerais, J., & Hecquet, M. (2016). Analysis of electromagnetically-induced vibrations of electrical machines

based on spatiogram technique. *International Journal of Applied Electromagnetics and Mechanics*, 51(1_suppl), S23-S32. https://doi.org/10.3233/JAE-2021.

[25] Wang, Z., Zhang, J., & Liang, Y. (2013). Motor noise and vibration test research. *TELKOMNIKA* (Telecommunication Computing Electronics and Control), 11(1), 87-94..

[26] Le Besnerais, J., Lanfranchi, V., Hecquet, M., Friedrich, G., & Brochet, P. (2007). Calcul du bruit acoustique d'une machine asynchrone a pas fractionnaire.

[27] Wang, C., Astfalck, A., & Lai, J. C. S. (2002). Sound power radiated from an inverter-driven induction motor: experimental investigation. IEE Proceedings-Electric Power Applications, 149(1), 46-52. https://doi.org/10.1049/ip-epa:20020067.

[28] Moysidis, D. A., Karatzinis, G. D., Boutalis, Y. S., & Karnavas, Y. L. (2023). A study of noise effect in electrical machines bearing fault detection and diagnosis considering different representative feature models. Machines, 11(11), 1029. https://doi.org/10.3390/machines11111029.

[29] Kester, W. (2009). Understand SINAD, ENOB, SNR, THD, THD+ N, and SFDR so you don't get lost in the noise floor. MT-003 tutorial, 01-08.

[30] Williamson, D. F., Parker, R. A., & Kendrick, J. S. (1989). The box plot: a simple visual method to interpret data. Annals of internal medicine, 110(11), 916-921. https://doi.org/10.7326/0003-4819-110-11-916.